B4GALNT3 regulates glycosylation of sclerostin and bone mass

Sofia Movérare-Skrtic,[a,*] Jakob Voelkl,[b,c,d] Karin H. Nilsson,[a] Maria Nethander,[a,e] Trang Thi Doan Luong,[b] Ioana Alesutan,[b] Lei Li,[a] Jianyao Wu,[a] Karin Horkeby,[a] Marie K. Lagerquist,[a] Antti Koskela,[f] Juha Tuukkanen,[f] Jon H. Tobias,[g] Ulf H. Lerner,[a] Petra Henning,[a] and Claes Ohlsson[a,h]

[a]Sahlgrenska Osteoporosis Centre, Centre for Bone and Arthritis Research, Institute of Medicine, Sahlgrenska Academy at University of Gothenburg, Gothenburg, Sweden
[b]Institute for Physiology and Pathophysiology, Johannes Kepler University Linz, Linz, Austria
[c]Department of Nephrology and Medical Intensive Care, Charité - Universitätsmedizin Berlin, Berlin, Germany
[d]DZHK (German Centre for Cardiovascular Research), Partner Site Berlin, Berlin, Germany
[e]Bioinformatics Core Facility, Sahlgrenska Academy, University of Gothenburg, Gothenburg, Sweden
[f]Department of Anatomy and Cell Biology, Faculty of Medicine, Institute of Cancer Research and Translational Medicine, University of Oulu, Oulu, Finland
[g]Musculoskeletal Research Unit, Translational Health Sciences, and Medical Research Council Integrative Epidemiology Unit, Bristol Medical School, University of Bristol, Bristol, UK
[h]Region Västra Götaland, Department of Drug Treatment, Sahlgrenska University Hospital, Gothenburg, Sweden

eBioMedicine
2023;91: 104546
Published Online xxx
https://doi.org/10.1016/j.ebiom.2023.104546

Summary

Background Global sclerostin inhibition reduces fracture risk efficiently but has been associated with cardiovascular side effects. The strongest genetic signal for circulating sclerostin is in the *B4GALNT3* gene region, but the causal gene is unknown. *B4GALNT3* expresses the enzyme beta-1,4-N-acetylgalactosaminyltransferase 3 that transfers N-acetylgalactosamine onto N-acetylglucosaminebeta-benzyl on protein epitopes (LDN-glycosylation).

Methods To determine if *B4GALNT3* is the causal gene, *B4galnt3*$^{-/-}$ mice were developed and serum levels of total sclerostin and LDN-glycosylated sclerostin were analysed and mechanistic studies were performed in osteoblast-like cells. Mendelian randomization was used to determine causal associations.

Findings *B4galnt3*$^{-/-}$ mice had higher circulating sclerostin levels, establishing B4GALNT3 as a causal gene for circulating sclerostin levels, and lower bone mass. However, serum levels of LDN-glycosylated sclerostin were lower in *B4galnt3*$^{-/-}$ mice. *B4galnt3* and *Sost* were co-expressed in osteoblast-lineage cells. Overexpression of *B4GALNT3* increased while silencing of *B4GALNT3* decreased the levels of LDN-glycosylated sclerostin in osteoblast-like cells. Mendelian randomization demonstrated that higher circulating sclerostin levels, genetically predicted by variants in the *B4GALNT3* gene, were causally associated with lower BMD and higher risk of fractures but not with higher risk of myocardial infarction or stroke. Glucocorticoid treatment reduced *B4galnt3* expression in bone and increased circulating sclerostin levels and this may contribute to the observed glucocorticoid-induced bone loss.

Interpretation B4GALNT3 is a key factor for bone physiology via regulation of LDN-glycosylation of sclerostin. We propose that B4GALNT3-mediated LDN-glycosylation of sclerostin may be a bone-specific osteoporosis target, separating the anti-fracture effect of global sclerostin inhibition, from indicated cardiovascular side effects.

Funding Found in acknowledgements.

Keywords: Osteoporosis; Osteoblasts; Fracture risk; Mendelian randomization

Introduction

Osteoporosis is a disease affecting millions of people worldwide.[1,2] Although the disability due to osteoporosis is enormous, the underlying mechanisms causing reduced bone mass and increased fracture susceptibility are not completely understood. Global sclerostin inhibition increases bone mass and reduces fracture risk efficiently but has in some, but not all, studies been associated with cardiovascular side effects.[3,4] Romosozumab is a monoclonal antibody against the Wnt inhibitor sclerostin, that is approved as an anabolic treatment of postmenopausal osteoporosis.[5] However,

*Corresponding author. Sahlgrenska Osteoporosis Centre, Centre for Bone and Arthritis Research, Institute of Medicine, Sahlgrenska Academy at University of Gothenburg, SE-41345 Gothenburg, Sweden.
E-mail address: sofia.skrtic@gu.se (S. Movérare-Skrtic).

Research in context

Evidence before this study

Global sclerostin inhibition is an approved osteoporosis treatment that reduces fracture risk efficiently but has been associated with cardiovascular side effects. Circulating sclerostin is derived from osteoblast-lineage cells. The strongest genetic signal for circulating sclerostin is in the *B4GALNT3* gene region, but the causal gene is unknown. The aim of the present study was to identify the causal gene for sclerostin levels in the *B4GALNT3* gene region and to establish how this gene regulates sclerostin levels. We hypothesized that methods targeting this mechanism may increase bone mass and reduce fracture risk without having cardiovascular side effects.

Added value of this study

This study showed that B4GALNT3 regulates bone mass and sclerostin levels via an enhanced specific glycosylation of sclerostin in osteoblast-lineage cells. Furthermore, we demonstrate that glucocorticoid-induced regulation of *B4galnt3* expression may contribute to glucocorticoid-induced bone loss. Finally, higher circulating sclerostin levels, genetically predicted by variants in the *B4GALNT3* gene, are causally associated with lower bone mineral density and higher risk of fractures, but not with higher risk of myocardial infarction or stroke in humans.

Implications of all the available evidence

B4GALNT3 is as a key factor for bone physiology via regulation of a specific glycosylation of sclerostin in osteoblast-lineage cells. B4GALNT3-mediated glycosylation of sclerostin may be a promising bone-specific osteoporosis target, separating anti-fracture effect from cardiovascular side effects.

as there is some evidence of potential cardiovascular safety concerns, recent myocardial infarction and stroke are contraindications for treatment using romosozumab. One Mendelian randomization (MR) study, using genetic variants in the *SOST* gene (coding for sclerostin) as exposure, revealed that the *SOST* SNPs alleles that display the strongest association with reduced fracture risk also associate with increased risk of myocardial infarction.[3] In contrast, another MR study using sclerostin SNPs strongly associated with *SOST* mRNA levels in vascular tissues as exposure did not observe an association with risk of myocardial infarction.[6] Furthermore, a protective role of sclerostin against vascular calcification was recently demonstrated using two mouse disease models.[7] Therefore, further studies determining the tissue-specific effects of sclerostin are warranted to either exclude cardiovascular side effects of global sclerostin inhibition or to develop alternative sclerostin-targeting therapies with a bone-specific effect, avoiding cardiovascular side effects.

Sclerostin is a glycoprotein mainly produced by late osteoblasts and osteocytes.[8] It exerts its main effect in bone where it plays an important role in the adaptive response to mechanical loading, acting within the local bone microenvironment to suppress bone formation in the absence of loading.[9] Circulating sclerostin is only derived from osteoblast-lineage cells as demonstrated by studies using mouse models with conditional inactivation of *Sost*.[10] Although high levels of sclerostin were found in the circulation of control mice, both a mouse model using *Col1-Cre* mediated deletion (inactivating genes in both osteoblasts and osteocytes), and a mouse model using *Dmp1-Cre* mediated deletion (inactivating genes in late osteoblasts/osteocytes) of sclerostin had no measurable levels of sclerostin in the circulation, clearly establishing that circulating sclerostin is only derived from late osteoblasts/osteocytes.[10] Nevertheless, SOST is also expressed in multiple non-bone tissues, including arteries, and may locally in these tissues exert important biological actions although these non-bone tissues do not have the capacity to contribute to circulating sclerostin levels.[11]

We recently observed that the strongest genetic signal for circulating sclerostin in humans is located on chromosome 12 in the *B4GALNT3* gene region, but the causal gene is unknown.[12] The aim of the present study was to identify the causal gene for sclerostin levels in the *B4GALNT3* gene region and to determine how this gene regulates sclerostin levels. We hypothesized that methods targeting this mechanism may increase bone mass and reduce fracture risk without having cardiovascular side effects.

Methods

Human genetic association studies

Look ups of signals for circulating sclerostin at the B4GALNT3 *gene region in different available data sets*

Femoral neck (FN)-BMD analysed by DXA. Associations with FN-BMD for the used SNPs at the *B4GALNT3* gene region are taken from the GWAS summary statistics from Zheng et al.,[12] available at the GEFOS website http://www.gefos.org.

Estimated BMD (eBMD) at the heel analysed by ultrasound. Associations with eBMD for the used SNPs at the *B4GALNT3* gene region are taken from the GWAS summary statistics from Morris et al.,[13] available at the GEFOS website http://www.gefos.org.

Fractures at any bone site. Association with fractures at any bone site for the used SNPs at the *B4GALNT3* gene

region are taken from the GWAS summary statistics for fractures at any bone site from Morris et al.,[13] available at the GEFOS website http://www.gefos.org.

Myocardial infarction. Association with myocardial infarction for the used SNPs at the *B4GALNT3* gene region are taken from the GWAS summary statistics from Hartiala et al.,[14] available at https://www.ebi.ac.uk/gwas/home.

Stroke. Association with stroke and ischemic stroke for the used SNPs at the *B4GALNT3* gene region are taken from the GWAS summary statistics for stroke and ischemic stroke from Malik et al.,[15] available at https://www.megastroke.org/.

New associations analyses for the used SNPs at the *B4GALNT3* gene region with distal forearm fractures

Our new analyses of associations between the used SNPs at the *B4GALNT3* locus with distal forearm fractures (defined by ICD10 codes S52.5 and S52.6; N = 7324 distal forearm fracture cases) were performed using data from the UK Biobank study (http://www.ukbiobank.ac.uk). Briefly, the UK Biobank is a large prospective cohort study of approximately a half million adult (ages 40–69 years) participants living in the United Kingdom, recruited from 22 centres across the United Kingdom in 2006–2010.[16] We included 438,756 participants of white European descent with valid data on the candidate SNPs at the *B4GALNT3* locus, the forearm fracture outcome, and relevant covariates (age, sex, height, weight). Associations between the used SNPs at the *B4GALNT3* locus and the forearm fracture outcome were performed using SAIGE.[17] Briefly, this method uses a scalable generalized mixed model region-based association test that can handle large sample sizes and accounts for unbalanced case–control ratios for binary traits. Fracture risk was corrected for age, age^2, height, weight, sex, genotyping array and PC1 + ... + PC20 in logistic regression models. Individuals were excluded based on unusually high heterozygosity or >5% missing genotype rate, a mismatch between self-reported and genetically inferred sex.

Selection of genetic instruments for circulating sclerostin in the *B4GALNT3* gene region

In total 69 genome-wide significant SNPs in the *B4GALNT3* gene region were identified in the GWAS for circulating sclerostin by Zheng et al.[12] Associations for these 69 SNPs are available in Table S1 of Zheng et al. We excluded 4 SNPs with P value > 5×10^{-8}. Of the remaining genetic variants, we selected those with the lowest P value having a pairwise squared correlation (r^2) less than 0.4, resulting in 10 validated genetic variants predicting circulating sclerostin to be used in the MR.[18]

We aligned the effect allele of each genetic variant on the circulating sclerostin increasing allele. Population-specific correlations between variants were estimated with LDlink[19] using the 1000 Genomes Project (phase 3) and the British in England and Scotland population. As described earlier, the selected SNPs had a pairwise r^2 less than 0.4[18] and they therefore contributed both common and unique information on circulating sclerostin. In the gene-based MR analyses, we subsequently accounted for remaining correlations among selected genetic variants; thereby this methodology captures the total cumulative unique but not overlapping association information with high precision from multiple SNPs within the *B4GALNT3* gene region.[20,21]

Mendelian randomization (MR)

We used a gene-based MR analysis to determine the causal associations of circulating sclerostin, genetically predicted by 10 variants in the *B4GALNT3* gene region, on BMD parameters, fracture risk, risk of myocardial infarction, risk of stroke and risk of ischemic stroke. As genetic variants are randomly distributed at birth, they are unaffected by confounders. Causal effect estimates were obtained using fixed effects inverse-variance weighted (IVW) that accounts for correlations among genetic variants within the evaluated gene region.[22,23] Heterogeneity would generally not be expected when using multiple variants in the same gene region that should have similar mechanisms of effect.[24] Even though we are using correlated variants from a single gene region we first used the Q statistic[25] to identify the presence of potential pleiotropy. As an additional tool to identify potential presence of directional pleiotropy, we used Egger regression accounting for correlated genetic variants.[23] All MR analyses were performed using the MendelianRandomization package in R, version 3.4.2.

Ethics

New analyses of associations between the SNPs at the *B4GALNT3* locus and distal forearm fractures were performed using data from the UK Biobank study. The UK Biobank has ethical approval from the North West Multi-Centre Research Ethics Committee (application no. 16/NW/0274), and informed consent was obtained from all participants. The present research was approved by the UK Biobank Research and Access Committee (application no. 51784).

Animal experiments

The experimental procedures involving animals were approved by the Ethics Committee in Gothenburg, Västra Götaland, and the care of the animals was in compliance with its guidelines. The mice were housed in a standard animal housing facility with a 12-h of darkness and a 12-h of light photoperiod. The temperature was controlled (22 °C) and food and water were available ad libitum.

Generation of B4galnt3$^{-/-}$ *mice*

Global *B4galnt3*$^{+/-}$ mice were generated by breeding heterozygous *B4galnt3*$^{tm1c(EUCOMM)Wtsi}$ male mice (Institut Clinique de la Souris, Illkirch, France), with female mice expressing cre recombinase ubiquitously and from an early embryonic stage under the control of the phosphoglycerate kinase-1 promoter (PGKcre).[26,27] In *B4galnt3*$^{tm1c(EUCOMM)Wtsi}$ mice, *LoxP* sites are introduced upstream from *B4galnt3* exon 8 and exon 10 (Fig. 1a). In *PGKcre*-expressing females, the cre activity starts in the diploid phase of oogenesis and thereby a complete recombination of *LoxP* sites occurs also in *cre*$^{-}$ offspring. In the presence of an active cre recombinase, the DNA fragment including exons 8–9 of the *B4galnt3* allele is excised and the offspring become *B4galnt3*$^{+/-}$ mice (Fig. 1a). Briefly, to generate *B4galnt3*$^{-/-}$, *B4galnt3*$^{+/-}$ and littermate *B4galnt3*$^{+/+}$ control mice for the experiments, *B4galnt3*$^{+/-}$ female and male mice were mated. The following primer pair was used for genotyping of the *B4galnt3*$^{-/-}$ mice: forward primer (5′-GGTGGCTTGCACATTCACAGGCG-3′) and reverse primer (5′-ACCCCTAGGGAGTTGACTGCTTGCC-3′), while the following primer pair was used for genotyping the *B4galnt3*$^{+/+}$ mice: forward primer (5′-GGTGGCTTGCACATTCACAGGCG-3′) and reverse primer (5′-TGGTAATTTGCCCAAAGTCGCCCAGG-3′). Detection of the presence of *PGKcre* was done using forward primer (5′-AACATGCTTCATCGTCGG-3′) and reverse primer (5′-TTCGGATCATCAGCTACACC-3′).

Glucocorticoid-treatment experiment

Twelve-wk-old female wild-type (WT) C57BL/6N mice were treated with a subcutaneous 60-day-slow-release pellet containing either prednisolone (7.6 mg × kg^{-1} × day^{-1}; Innovative Research of America, Sarasota, FL) or vehicle for four weeks. This prednisolone dose has in previous studies been shown to exert effects on the skeleton in mice.[28] The pellets were inserted under anaesthesia with isoflurane (Baxter Medical AB, Kista, Sweden) and Rimadyl (Orion Pharma AB, Animal Health, Sollentuna, Sweden) was given as an analgesic.

At termination, the mice were anesthetized with Ketador/Dexdomitor (Richter Pharma/Orion Pharma), bled, and euthanized by cervical dislocation. Long bones and vertebrae were dissected and stored for future analyses, soft tissues were collected, weighed, and snap-frozen in liquid nitrogen.

Measurement of serum sclerostin

Blood samples were collected at termination and the serum was separated and kept at –80 °C until analysis. Serum levels of sclerostin were measured using a commercially available ELISA (ALPCO immunoassays, Salem, NH).

Assessment of bone parameters

Dual-energy X-ray absorptiometry (DXA)

Analyses of total body areal bone mineral density (aBMD), lumbar spine aBMD (L2–L5), and whole femur aBMD were performed using Faxitron UltraFocus DXA (Faxitron Bioptics, Tuscon, AZ). The DXA analyses were performed under anaesthesia by intraperitoneal injection of Ketanest/Dexdomitor (Pfizer/Orion Pharma).

High resolution micro computed tomography (μCT)

High resolution micro computed tomography (μCT) was used to analyse lumbar vertebra 5 and tibia (Skyscan, 1172; Bruker MicroCT, Aartselaar, Belgium), as previously described.[29] The lumbar vertebra and tibia were imaged with an X-ray tube voltage of 50 kV and a current of 201 μA, with a 0.5 mm aluminium filter, and the scanning angular rotation was 180°, and the angular increment was 0.70°. NRecon (version 1.6.9.8, Bruker MicroCT) was used to perform reconstruction after scans. In the vertebra, the trabecular bone was analysed 235 μm from the lower end of the pedicles and continued for approximately 229 μm. In the tibia, the trabecular bone distal to the proximal growth plate was selected for analysis within a conforming volume of interest (cortical bone excluded), commencing at a distance of 650 μm from the growth plate and extending a further longitudinal distance of 134 μm in the distal direction. The data was analysed using the CTAn software (version 1.13.2.1, Bruker MicroCT).

Peripheral quantitative computed tomography (pQCT)

Peripheral quantitative computed tomography (pQCT) was performed on tibia using pQCT XCT Research M (version 4.5B; Norland) at a resolution of 70 μm, as previously described.[30,31] Cortical bone was determined with a mid-diaphyseal scan positioned distal from the proximal growth plate of the tibia, corresponding to 30% of the bone length.

Mechanical strength

After dissection, the humerus was frozen at –20 °C. Three-point bending was performed with a span length of 4.5 mm and a loading speed of 0.155 mm/s using an Instron 3366 (Instron, Norwood, MA). Biomechanical parameters, based on the recorded load deformation curves, were calculated from Bluehill 2 software v.2.6 (Instron) with custom-made Excel (Microsoft, Redmond, WA) macros.[29]

RNA isolation, cDNA synthesis and quantitative real-time PCR analyses of mice tissue and primary periosteal cells

Total RNA was prepared from mouse cortical bone, aorta, and kidney and primary periosteal cells using Trizol reagent (Thermo Fisher Scientific) and/or RNAeasy micro kit in a Qiacube preparation robot (Qiagen). The mRNA was reversed transcribed to cDNA (Thermo Fisher

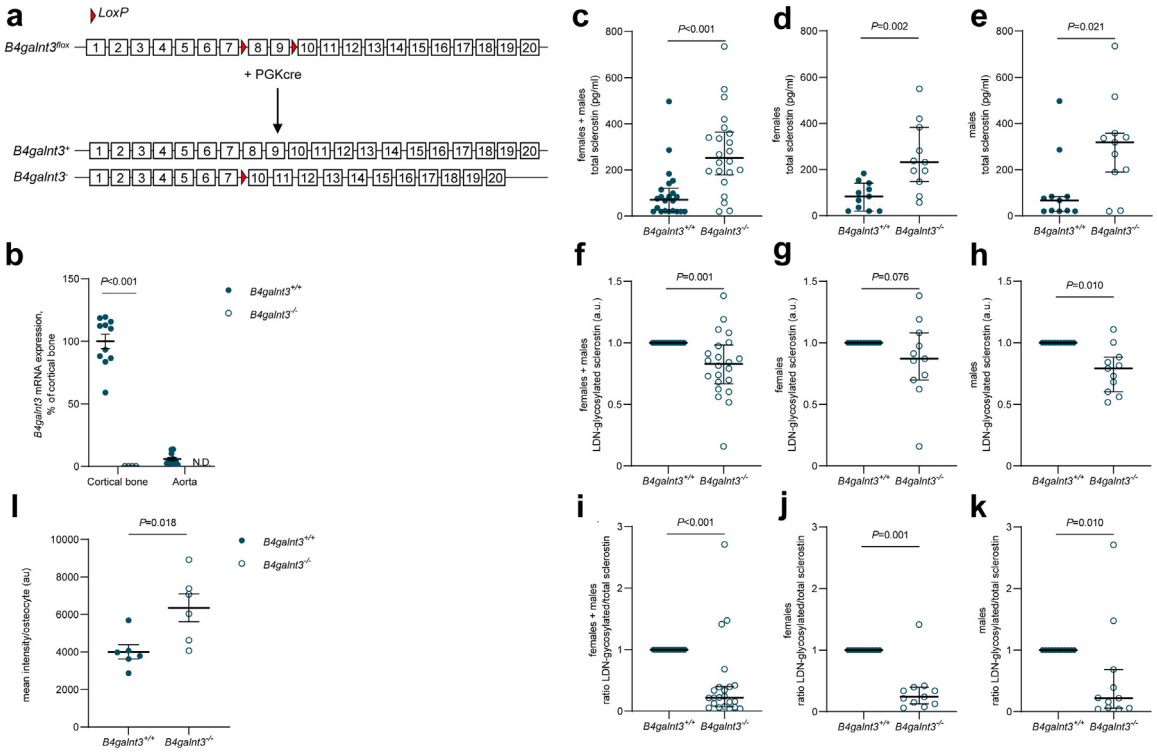

Fig. 1: B4galnt3$^{-/-}$ mice have increased levels of total serum sclerostin but decreased levels of LDN-glycosylated sclerostin in serum. a) Schematic illustration of the *B4galnt3* inactivated mouse model. The *B4galnt3* gene has 20 exons and the two *LoxP* sites are located in the introns upstream of exons 8 and 10. b) mRNA expression analyses of *B4galnt3* in the cortical bone of tibia and aorta in 13-wk-old female *B4galnt3*$^{+/+}$ mice (n = 11) and *B4galnt3*$^{-/-}$ homozygote (n = 12) mice. Individual values are presented with the mean as horizontal lines and ±SEM as vertical lines. Statistical analyses were performed using two-sided Student's *t* test. ND = not detectable. c–e) Total serum sclerostin levels in female + male (c), female (d), and male (e) *B4galnt3*$^{+/+}$ and *B4galnt3*$^{-/-}$ mice (female *B4galnt3*$^{+/+}$ n = 11; female *B4galnt3*$^{-/-}$ n = 11; male *B4galnt3*$^{+/+}$ n = 11; male *B4galnt3*$^{-/-}$ n = 11) as measured by ELISA. Values are given as medians and interquartile range. Statistical analyses were performed using two-sided Student's *t* test. f–h) Normalized LDN-glycosylated sclerostin protein levels from serum of female + male (f), female (g), and male (h) *B4galnt3*$^{+/+}$ and *B4galnt3*$^{-/-}$ mice (female *B4galnt3*$^{+/+}$ n = 11; female *B4galnt3*$^{-/-}$ n = 11; male *B4galnt3*$^{+/+}$ n = 11; male *B4galnt3*$^{-/-}$ n = 11) after precipitation with *Wisteria floribunda* agglutinin (WFA) agarose beads and analysed by Western blot. On each Western blot (see example in Supplemental Figure S2a and b), serum from one random *B4galnt3*$^{+/+}$ and one random *B4galnt3*$^{-/-}$ mice with and without WFA in the precipitation were included and the levels in *B4galnt3*$^{-/-}$ mouse were normalized to the levels in the *B4galnt3*$^{+/+}$ mouse set to 1. Values are given as medians and interquartile range. Statistical analyses were performed on normalized data using Mann–Whitney U-test. i–k) Ratio of LDN-glycosylated/total sclerostin levels in female + male (i), female (j), and male (k) *B4galnt3*$^{+/+}$ and *B4galnt3*$^{-/-}$ mice (female *B4galnt3*$^{+/+}$ n = 11; female *B4galnt3*$^{-/-}$ n = 11; male *B4galnt3*$^{+/+}$ n = 11; male *B4galnt3*$^{-/-}$ n = 11). The ratio in a *B4galnt3*$^{-/-}$ mouse was normalized to the ratio in the *B4galnt3*$^{+/+}$ mouse analysed on the same Western blot. Values are given as medians and interquartile range. Statistical analyses were performed on normalized data using Mann–Whitney U-test. l) Quantification of the intensity of sclerostin immunoreactivity per osteocyte in tibia. Results are expressed as mean intensity per osteocyte (male *B4galnt3*$^{+/+}$ mice n = 6; *B4galnt3*$^{-/-}$ mice n = 6). Individual values are presented with the mean as horizontal lines and ±SEM as vertical lines. Statistical analyses were performed using two-sided Student's *t* test. The results refer to 13-week-old *B4galnt3*$^{+/+}$ and *B4galnt3*$^{-/-}$ mice. LDN = LacdiNAc.

Scientific) and real-time PCR analyses were performed using the StepOnePlus Real-Time PCR System (version 2.3, Thermo Fisher Scientific). Expression of *B4galnt3* mRNA was analysed by use of custom-made primers and probe spanning the exon 8–9 boundary: forward primer: 5′-ATCAGCCTCCCTCAGGTACT-3′; reverse primer: 5′-AACTTGGCTCCAGGGTCATT-3′; and probe: FAM-5′-CCACGCGACCTCCACGTGGT-3′. The following Assay-on-Demand primer and probe sets were used: *sclerostin (Sost)*, Mm00470479_m1; *osteocalcin (Bglap)*, Mm03413826_mH; *osteopontin (Spp1)*, Mm00436767_m1; *OPG (Tnfrsf11b)*, Mm00435452_m1; *Nfatc1*, Mm00479445_m1; *αKlotho*, Mm00502002_m1; *Runx2*, Mm00501580_m1; *Axin2*, Mm00443610_m1; *Lef1*, Mm01310389_m1; *Tcf7 (Tcf1)*, Mm00493445_m1; *Cyclin D1 (Ccnd1)*, Mm00432359_m1; and *B4galnt4*, Mm01276749_g1. The relative gene expression was calculated by $2^{-\Delta\Delta Ct}$ method using the expression of the 18S ribosomal subunit (4310893E; Thermo Fisher Scientific) as internal standard.

In situ hybridization

The chromogenic *in situ* hybridization (cISH) was performed by using the RNAscope Duplex Detection Kit (322500, Advanced Cell Diagnostics (ACD), Bio-Techne Ltd., Abingdon, UK). Briefly, the bone specimens were fixated in 4% formaldehyde in phosphate buffered saline for 24 h and demineralized in 15% EDTA with 0.4% PFA for three weeks. The tissues were embedded with paraffin and sectioned at 6-µm thickness. After deparaffinization, standard RNAscope protocols were applied according to manufacturer's instructions with minor modifications, as described below. Rehydrated sections were blocked by kit-provided hydrogen peroxide and heated in target retrieval buffer, then digested by 10% pepsin. cISH target probes were applied and incubated overnight at 40 °C. The following probes were used: Mm-B4galnt3 (ACD; 857461), Mm-Dmp1 (ACD; 441171-C2), Mm-Sost (ACD; 410031-C2), Mm-Ctsk (ACD; 464071-C2) and Mm-Runx2 (ACD; 414021-C2). During/after ten steps of amplification, the signals were visualized by kit-provided fast red (C2 channel) and green (C1 channel) dyes and sections were counterstained with 50% haematoxylin. Images were captured on a Nikon Eclipse 80i light microscope. The number of *B4galnt3*-positive osteocytes was quantified in tibia of female mice and was expressed as a mean value of three sections from the proximal, middle, and distal tibia (n = 5 mice). Statistical analyses were performed using two-sided Student's *t* test.

Immunofluorescence

Dissected tibiae were fixated in 4% formaldehyde in phosphate buffered saline for 48 h and demineralized in 10% EDTA for four weeks, embedded in paraffin and longitudinal sectioned at 4-µm thickness. Immunofluorescence staining was applied with SOST antibody (1:50, R&D, AF1589) overnight at 4 °C. The sections were then incubated with Alexa 647-conjugated secondary antibody (1:400, Jackson ImmunoResearch, 705-605-003) for 2 h at RT, followed by counterstaining with DAPI for 10 min. The images were captured by the spinning-disk confocal microscope (Nikon). 3–5 slices were picked from each mouse, 1–2 images were taken from each slice and >100 DAPI positive cells in the cortical bone were counted in each image. The quantification of SOST positive cells and the measurement of the fluorescence intensity were performed by NIS-Elements and ImageJ.

Cell culture of Saos-2 cells

Saos-2 cells (ATCC) were routinely cultured in McCoy's 5A medium supplemented with 15% FBS (Fisher Scientific), 100 U/mL penicillin (Fisher Scientific) and 100 µg/mL streptomycin (Fisher Scientific). Where indicated, Saos-2 cells were transfected with 2 µg DNA encoding human *B4GALNT3* in pcDNA3.1 vector (GenScript) or empty vector as control using X-tremeGENE HP DNA transfection reagent (Roche Applied Science). Saos-2 cells were transfected with 10 nM human *B4GALNT3* siRNA (ID no. s49202) or 10 nM negative control siRNA (ID no. 4390843) using siPORT amine transfection agent (all from Fisher Scientific). Saos-2 cells were used 48 h following transfection and transfection efficiency was determined by real-time PCR.

RNA isolation, cDNA synthesis and quantitative real-time PCR analyses of Saos-2 cells

Total RNA was isolated from Saos-2 cells by using Trizol Reagent (Fisher Scientific). cDNA was synthesized with SuperScriptIII Reverse Transcriptase and oligo(dT)$_{12–18}$ primers (Fisher Scientific). RT-PCR was performed in duplicate with iQ™ Sybr Green Supermix (Bio-Rad Laboratories) and CFX96 Real-Time PCR Detection System (Bio-Rad Laboratories). The following human primers were used (Fisher Scientific): *B4GALNT3* forward primer: 5′-TGGCAGCTCTATCCAGCAG-3′; *B4GALNT3* reverse primer: 5′-GCCATAGTTGGTCCATTTGGG-3′; *GAPDH* forward primer: 5′-GAGTCAACGGATTTGGTCGT-3′; *GAPDH* reverse primer: 5′-GACAAGCTTCCCGTTCTCAG-3′; *SOST* forward primer: 5′-ACACAGCCTTCCGTGTAGTG-3′; *SOST* reverse primer: 5′-GGTTCATGGTCTTGTTGTTCTCC-3′. The specificity of the PCR products was confirmed by analysis of the melting curves. Relative mRNA expression was calculated by the $2^{-\Delta\Delta Ct}$ method using GAPDH as housekeeping gene, normalized to the control group.

Measurements of LDN-glycosylated sclerostin

B4GALNT3 form a LacdiNAc (LDN) disaccharide determinant on target glycoproteins.[32] To quantify the amount of sclerostin carrying a LDN, *Wisteria floribunda* agglutinin (WFA) agarose beads were used for precipitation.[33] WFA is a legume lectin that recognizes and preferentially binds the disaccharide LDN with high affinity.[34] Briefly, Saos-2 cells were lysed with ice-cold IP lysis buffer supplemented with complete protease and phosphatase inhibitors cocktail (Fisher Scientific) and total protein concentration was measured by the Bradford assay (Bio-Rad Laboratories). Precipitation was performed from 25 µL human serum collected from healthy volunteers,[35] from 2 Ll serum of *B4galnt3*$^{-/-}$ and corresponding *B4galnt3*$^{+/+}$ female and male mice, or from 100 µg of Saos-2 cells total proteins, with the WFA agarose beads (Vector Laboratories) and control agarose beads by using Pierce Classic IP kit (Fisher Scientific). The eluted proteins following precipitation were separated on SDS-polyacrylamide gels and transferred to PVDF membranes. The membranes were incubated with primary rabbit anti-sclerostin antibody (1:1000, Abcam) at 4 °C overnight and then with secondary anti-rabbit HRP-conjugated antibody at room temperature for 1 h (1:1000, Cell Signaling). Bands were detected with Clarity Western ECL substrate (Bio-Rad Laboratories) and ChemiDoc MP

imaging system (Bio-Rad Laboratories) and quantified by using ImageJ software.

Single cell RNA sequencing (scRNAseq)

The expression of *B4galnt3* and *Sost* in bone marrow cells were investigated in two different publicly available scRNAseq datasets as previously described.[36,37] The online nichExplorer made available by Iannis Aifantis laboratory (http://aifantislab.com/niche) was used to study expression in mouse bone marrow vascular (*VE-Cad*$^{+}$), perivascular (*Lepr*$^{+}$), and osteoblast (*Col2.3*$^{+}$) cell populations. Datasets published by Matsushita et al.[38] were used to study the expression in *Cxcl12*$^{+}$ bone marrow stromal cells.

Primary calvarial osteoblast cultures

Primary periosteal cells were isolated from calvarial bones from 3 to 5 days old C57BL/6N mice by sequential collagenase treatment as previously described.[39] Cells from collagenase fractions 6–10 were cultured for 2–3 days in MEMalpha medium (Gibco, cat no 22561-021) supplemented with 10% heat inactivated fetal bovine serum (Sigma, cat no F7525), 50 μg/mL gentamicin (Gibco, cat no 15750-037), PEST (100 U/mL penicillin, 100 μg/mL streptomycin, Gibco, cat no 15140-148) and 2 mM GlutaMAX (Gibco, cat no 35050-038), before detachment with trypsin and re-seeding at a density of 20,000 cells/cm^2 in osteogenic media (MEMalpha with above supplements and 4 mM beta-glycerophosphate, Sigma cat no G9422, and 0.28 mM ascorbic acid, Sigma cat no A8960), with and without 100 nM dexamethasone (Sigma, cat no D4902). After 48 h the cells were harvested and RNA isolated using the RNeasy Micro kit according to the instructions from the manufacturer (Qiagen, cat no 74004).

Statistics

The predesigned primary endpoint in the mouse studies was to record the effect of *B4galnt3* inactivation on cortical bone area. Our power analysis suggested that when using eight WT and eight *B4galnt3*$^{-/-}$ mice, we would have 80% power to detect a biological significant effect with a 1.51 SD change in cortical bone area, and therefore we aimed to use at least eight mice per group in the different mouse studies. No animal experiments requiring randomization of sample groups were performed. All animals of the required genotype were included in the experiments. Exclusion criteria were technical failure at analysis. For normally distributed data, two-sided Student's *t* test was used and for non-parametric data, Mann–Whitney U-test was used. Spearman correlation analysis was used to assess the relationship between serum sclerostin and cortical bone area in the tibia of *B4galnt3*$^{-/-}$ mice and WT mice. A P value < 0.05 was considered statistically significant.

Role of funding source

The funders played no role in the design of the research, collection, analysis and interpretation of data, the writing of the paper or the decision to submit the manuscript for publication.

Results

B4GALNT3 reduces circulating sclerostin via glycosylation of sclerostin in osteocytes/late osteoblasts

We have previously demonstrated that the A allele of the rs215226 SNP in the *B4GALNT3* gene region on chromosome 12 is robustly associated with increased circulating levels of sclerostin in humans.[12] To determine if B4GALNT3 is the causal gene for the strong association signal for circulating sclerostin at the *B4GALNT3* locus, we first developed a mouse model with global inactivation of *B4galnt3* (Fig. 1a). *B4galnt3*$^{-/-}$ mice were born healthy and according to Mendel's law of inheritance and had normal body weight and relative organ weights of kidney, spleen, gonadal fat, retroperitoneal fat, uterus, and seminal vesicles (Supplemental Table S1). Analysis of the *B4galnt3* mRNA expression in bone, aorta and kidney confirmed that the *B4galnt3* gene was inactivated in *B4galnt3*$^{-/-}$ mice (Fig. 1b, Supplemental Figure S1b).

Importantly, the serum sclerostin levels were substantially increased in *B4galnt3*$^{-/-}$ mice compared with littermate control mice (Fig. 1c–e; females + males (Fig. 1c): +185%, $P < 0.001$, two-sided Student's *t* test), reminiscent of the results of the A allele of rs215226 in humans. As *B4GALNT3* expresses the enzyme beta-1,4-N-acetylgalactosaminyltransferase 3 that transfers N-acetylgalactosamine (GalNAc) onto N-acetylglucosaminebeta-benzyl to form GalNAcβ1,4-GlcNAc structures on protein epitopes (LDN-glycosylation),[40] we compared the levels of LDN-glycosylated sclerostin between *B4galnt3*$^{-/-}$ and littermate *B4galnt3*$^{+/+}$ control mice. The LDN-glycosylated sclerostin was analysed by *W. floribunda* agglutinin (WFA; recognizes and preferentially binds LDN-glycosylation with high affinity[34]) precipitation, followed by sclerostin Western blot analysis. In contrast to total levels of sclerostin, both the level of LDN-glycosylated sclerostin (Fig. 1f–h; females + males (Fig. 1f): $P = 0.001$, Mann–Whitney U-test, Supplemental Fig. S2a and b) and the LDN-glycosylated sclerostin/total sclerostin ratio (Fig. 1i–k; females + males (Fig. 1i): $P < 0.001$, Mann–Whitney U-test) in the circulation were reduced in *B4galnt3*$^{-/-}$ mice compared with littermate *B4galnt3*$^{+/+}$ control mice. WFA precipitation followed by Western blot analysis revealed that LDN-glycosylated sclerostin was present also in human serum (Supplemental Figure S2c). The intensity of sclerostin immunoreactivity per osteocyte in cortical diaphyseal bone was

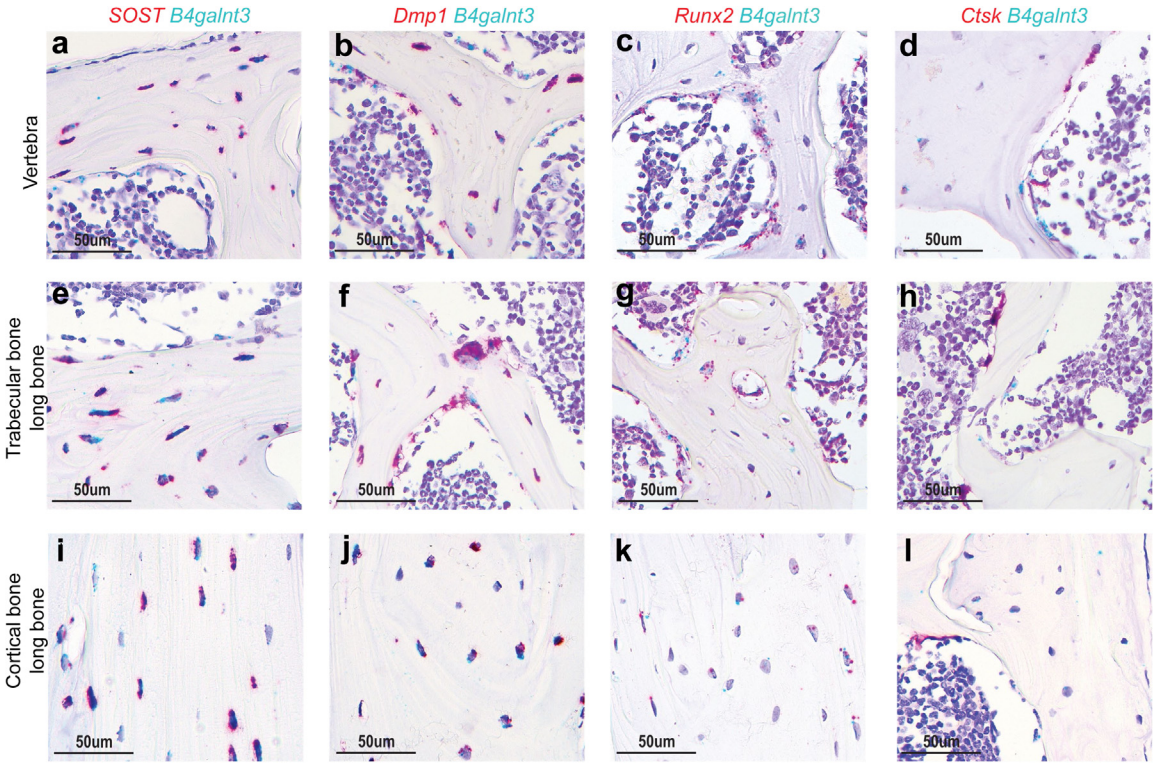

***Fig. 2: B4galnt3* is expressed in osteoblasts and osteocytes but not in osteoclasts.** a–l) Representative *in situ* hybridization images in mice. Transverse sections across lumbar vertebra 5 (a–d) and longitudinal sections of femur or tibia (e–l) in mice demonstrate the mRNA expression of *B4galnt3* (blue; a–l) and *Sost* (red; a, e, i), *Dmp1* (red; b, f, j), *Runx2* (red; c, g, k) or *Ctsk* (red; d, h, l). *B4galnt3* mRNA could be observed in *Sost*-, *Dmp1*-, and *Runx2*-expressing osteocytes and osteoblast- lineage cells on the bone surface. In contrast, *B4galnt3* was not detectable in *Ctsk*-expressing osteoclasts. Scale bar 50 µm. Images are representative of at least three independent experiments.

increased in *B4galnt3*$^{-/-}$ mice compared with WT mice (Fig. 1l and Supplemental Figure S1c).

Besides B4GALNT3, also B4GALNT4, has been shown to have the capacity to synthesize LDN-glycosylation structures.[32,40,41] *B4galnt4* was expressed in the cortical bone of *B4galnt3*$^{-/-}$ mice but its expression did not differ between *B4galnt3*$^{-/-}$ and WT mice (Supplemental Table S2).

As previous studies using inactivation of *Sost* specifically in DMP1-expressing cells have revealed that circulating sclerostin is completely derived from osteocytes/late osteoblasts in mice[10] and the enzymatic post-translational action of B4GALNT3 with an impact on circulating sclerostin levels is exerted intracellularly in the cells secreting sclerostin, we hypothesize that B4GALNT3 increases LDN-glycosylation of sclerostin in osteocytes/late osteoblasts and that this, in turn, reduces circulating sclerostin via an increased degradation locally in bone and/or reduced half-life of circulating LDN-glycosylated sclerostin compared with sclerostin without a LDN-glycosylation.

To determine the localization of the cells expressing *B4galnt3* within the skeleton, chromogenic *in situ* hybridization was performed (Fig. 2a–l). *B4galnt3* was detected in *Runx2*- and *Dmp1*-expressing osteoblasts on the trabecular surfaces and in *Dmp1*-expressing osteocytes in the trabecular bone of the vertebra (Fig. 2b and c). In the long bones, *B4galnt3* mRNA was detected in *Runx2*- and *Dmp1*-expressing osteoblasts on the trabecular surfaces (Fig. 2f and g) as well as in *Dmp1*-expressing osteocytes in cortical bone (Fig. 2j). Counting the proportion of *B4galnt3* expressing osteocytes in the cortical bone revealed that 34.8 ± 1.4% (mean ± standard error of the mean, n = 5) of the osteocytes were *B4galnt3*-positive. Combined chromogenic *in situ* hybridization revealed that *B4galnt3* was colocalized with *Sost* in osteocytes and late osteoblasts (Fig. 2a, e, and i). We also determined if *B4galnt3* and *Sost* are co-expressed in mesenchymal stem cells in the bone marrow. Two independent single cell RNA-sequencing (scRNAseq) data sets of bone marrow cells[38,42] were evaluated but neither *B4galnt3* nor *Sost* were expressed in bone marrow stromal cells expressing early osteoblastic markers (Supplemental Figure S3). In addition, no *B4galnt3* mRNA expression was detected in *Ctsk*-expressing osteoclasts (Fig. 2d, h, and l). Thus, circulating sclerostin is derived from osteocytes/late osteoblasts and *B4galnt3* and *Sost* are co-expressed in

these cells. Normal *Sost* expression was observed in bone of *B4galnt3*$^{-/-}$ mice (Supplemental Figure S1b), demonstrating that the B4GALNT3-mediated regulation of circulating sclerostin is not caused by a transcriptional regulation of *Sost* in late osteoblasts/osteocytes. The expression of *B4galnt3* in mice was –96% lower in aorta compared with cortical bone (Fig. 1b). The *B4GALNT3* mRNA expression was also modest in the aorta when compared with the expression in multiple tissues (n = 54) available at the GTEx portal (https://gtexportal.org/home/; Supplemental Figure S4a). In contrast, the *SOST* expression in aorta was highest among all tissues available at the GTEx portal (Supplemental Figure S4b; bone not available at the GTEx portal). Thus, the expression of both *SOST* and *B4GALNT3* is relatively high in cortical bone. In contrast, *SOST* but not *B4GALNT3* expression is high in aorta. These expression patterns indicate that SNPs affecting *SOST* expression will have an impact on both bone and aorta while SNPs affecting *B4GALNT3* expression may preferentially have an impact on LDN-glycosylation of sclerostin in bone.

We next determined if B4GALNT3 contributes to post-translational modification by regulating LDN-glycosylation of sclerostin in human osteoblast-like osteosarcoma Saos-2 cells, expressing both *B4GALNT3* mRNA and *SOST* mRNA. First, to determine if reduction of *B4GALNT3* expression in osteoblast-like cells regulates LDN-glycosylation of sclerostin, *B4GALNT3* expression was silenced in the human osteoblast-like cell line Saos-2. Expression of *B4GALNT3* mRNA was substantially reduced in the *B4GALNT3* silenced Saos-2 cells compared with Saos-2 cells transfected with a negative control siRNA (Fig. 3a), whereas the mRNA expression of *SOST* was unchanged (Fig. 3b). Subsequent WFA precipitation followed by Western blot analysis demonstrated a reduction in the LDN-glycosylated sclerostin levels in the *B4GALNT3* silenced Saos-2 cells compared with Saos-2 cells transfected with a negative control siRNA (Fig. 3c and d). These results demonstrate that B4GALNT3 enhances post-translational LDN-glycosylation of sclerostin while *SOST* transcription is not affected by B4GALNT3 in osteoblast-like cells.

Second, Saos-2 cells were transfected with DNA encoding the human *B4GALNT3* gene in a vector or an empty control vector. Real-time PCR analyses revealed an increase in *B4GALNT3* expression in the *B4GALNT3* overexpressing Saos-2 cells compared with Saos-2 cells transfected with an empty vector (Fig. 3e), whereas the mRNA expression of *SOST* was unchanged (Fig. 3f). WFA precipitation followed by Western blot analysis showed a significant increase in LDN-glycosylated sclerostin levels in the *B4GALNT3* overexpressing Saos-2 cells compared with Saos-2 cells transfected with an empty vector (Fig. 3g and h).

Human genetic analyses of the causal effects of genetic variants in the *B4GALNT3* gene region

One previous Mendelian randomization (MR) study, using genetic variants in the *SOST* gene as exposure, revealed that the *SOST* SNPs alleles that display the strongest association with reduced fracture risk also associate with increased risk of myocardial infarction.[3] After having demonstrated that *B4GALNT3* is the causal gene for the observed strong association between SNPs in the *B4GALNT3* gene region and circulating levels of sclerostin, we determined the causal association for B4GALNT3-regulated circulating sclerostin levels with bone health parameters and risk of myocardial infarction in humans. Two-sample MR studies using gene-based genetic instruments assessed the causal association between circulating sclerostin genetically predicted by 10 variants in the *B4GALNT3* gene region and bone mineral density (BMD), risk of fractures and risk of myocardial infarction. Using IVW MR adjusted for SNP correlations, we observed that circulating sclerostin genetically predicted by variants in the *B4GALNT3* gene region was inversely associated with estimated (e)BMD, as analysed by ultrasound in the heel, and femoral neck BMD, as analysed by DXA (Table 1, Supplemental Table S3). In addition, increased circulating sclerostin, genetically predicted by variants in the *B4GALNT3* gene region, was causally associated with increased risk of fractures at any bone site (OR 1.10, 95% CI 1.03–1.17 per SD increase in sclerostin) and substantially increased risk of distal forearm fractures (OR 1.25, 95% CI 1.06–1.48 per SD increase in sclerostin; Table 1, Supplemental Table S3). Using the largest available GWAS data set for myocardial infarction (61,000 myocardial infarctions and 577,000 controls[14]), we evaluated the association between circulating sclerostin predicted by 10 variants in the *B4GALNT3* gene region and risk of myocardial infarction. No trend of causal association was observed in the IVW analyses for myocardial infarction (Table 1, Supplemental Table S3). However, MR Egger analyses revealed that the Egger intercept was significant, indicating pleiotropy, implying that the slope from the Egger regression should be considered. The Egger slope revealed a significant direct association between sclerostin levels genetically predicted by variants in the *B4GALNT3* gene region and risk of myocardial infarction (OR 1.14, 95% CI 1.03–1.25 per SD increase in sclerostin: Table 1, Supplemental Table S3). Thus, genetic variants in the *B4GALNT3* gene region that increase BMD and reduce fracture risk might reduce (and not increase) risk of myocardial infarction. Finally, our MR analyses revealed that circulating sclerostin, genetically predicted by variants in the *B4GALNT3* gene region, was not causally associated with risk of stroke or ischemic stroke (Table 1, Supplemental Table S4).

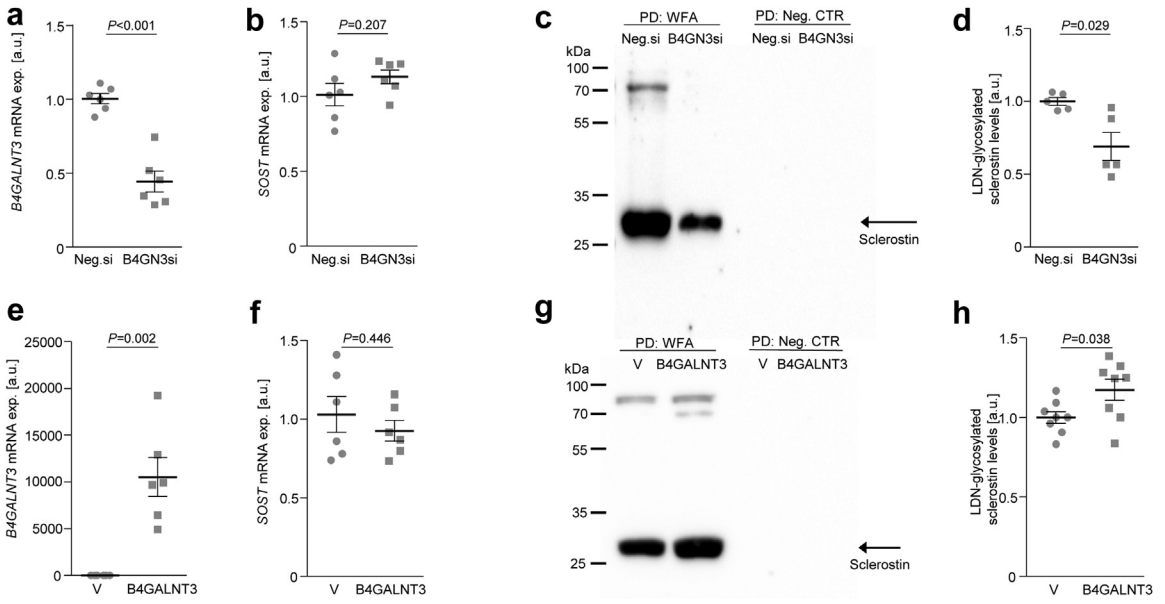

Fig. 3: **B4GALNT3 contributes to post-translational modification by regulating LDN-glycosylation of sclerostin in human osteoblast-like cells.** a and b) *B4GALNT3* (a) and *SOST* (b) mRNA expression in Saos-2 cells following transfection with negative control siRNA (Neg.si) or B4GALNT3 siRNA (B4GN3si) (n = 6 per group). Values are given as means ± SEM. Statistical analyses were performed using two-sided Student's *t* test. c) Representative Western blot showing LDN-glycosylated sclerostin protein levels after precipitation with WFA agarose beads or negative control (Neg. CTR) agarose beads from Saos-2 cells following transfection with negative control siRNA (Neg.si) or B4GALNT3 siRNA (B4GN3si). d) Normalized quantification of LDN-glycosylated sclerostin protein levels after precipitation with WFA agarose beads from Saos-2 cells following transfection with negative control siRNA (Neg.si) or B4GALNT3 siRNA (B4GN3si) and detected by Western blot analysis (n = 5 per group). Values are given as means ± SEM. Statistical analyses were performed on normalized data using two-sided Student's *t* test. e and f) *B4GALNT3* (e) and *SOST* (f) mRNA expression in Saos-2 cells following transfection with empty vector (V) or a construct encoding human *B4GALNT3* (n = 6 per group). Values are given as means ± SEM. Statistical analyses were performed using Mann–Whitney U-test for (e) and two-sided Student's *t* test for (f). g) Representative Western blot showing LDN-glycosylated sclerostin protein levels after precipitation with WFA agarose beads or negative control (Neg. CTR) agarose beads from Saos-2 cells following transfection with empty vector (V) or a construct encoding human *B4GALNT3*. h) Normalized quantification of LDN-glycosylated sclerostin protein levels after precipitation with WFA agarose beads from Saos-2 cells following transfection with empty vector (V) or a construct encoding human *B4GALNT3* and detected by Western blot analysis (n = 8 per group). Values are given as means ± SEM. Statistical analyses were performed on normalized data using two-sided Student's *t* test. LDN = LacdiNAc, PD = precipitation, WFA = *Wisteria floribunda* agglutinin, a.u. = arbitrary units.

Genetic variants in *SOST* and *B4GALNT3* are independently associated with BMD

We next determined the combined impact of a genetic variant in *BGALNT3* (top SNP rs215226), reflecting post-translational LDN-glycosylation of sclerostin, and two genetic variants in *SOST* (G allele in rs7209826 and A allele in rs188810925), reflecting *SOST* expression on eBMD.[3] All three SNPs were strongly associated with eBMD in the UK Biobank (Supplemental Table S5) in age and sex adjusted models. Combined models including one of the two *SOST* SNPs and SNP rs215266 in *B4GALNT3* revealed that the *B4GALNT3* SNP rs215226 and the two *SOST* SNPs are independently associated with eBMD (Supplemental Table S5). The associations for *B4GALNT3* and *SOST* SNPs were additive as illustrated in Supplemental Figures S5 and S6 while no significant interaction between SNPs in *B4GALNT3* and *SOST* for this association was observed (*P* values for SNP × SNP interactions were all >0.05). These findings indicate that alteration of sclerostin expression (indicated by SNPs regulating *SOST* transcription) and post-translational LDN-glycosylation of sclerostin (indicated by the *B4GALNT3* SNP) may exert additive effects on bone mass.

Hormonal regulation of *B4GALNT3* expression in bone

As B4GALNT3 influences both sclerostin levels, and bone mass, we hypothesized that hormones regulating bone mass might exert their effects on bone, at least partly, via modulation of *B4GALNT3* expression in bone. Glucocorticoid (GC)-treatment reduces BMD and increases fracture risk, and GC-induced bone loss is not observed in $Sost^{-/-}$ mice,[43] suggesting that modulation of sclerostin levels/activity is involved in GC-induced bone loss. To determine if GC-induced bone loss is associated with changes in *B4GALNT3* expression in bone, and thereby sclerostin levels, we treated mice with

	Beta	SE	*P* value	N subjects		Source
Bone parameters						
eBMD	−0.12	0.01	4.0E-38	426,824		Morris et al.[13]
FN-BMD	−0.08	0.04	2.1E-02	53,236		Zheng et al.[12]
Binary outcomes	**OR**	**95% CI**	***P* value**	**N cases**	**N controls**	
Fractures						
Fracture at any bone site	1.10	(1.03–1.17)	2.9E-03	53,184	426,795	Morris et al.[13]
Distal forearm fractures	1.25	(1.06–1.48)	7.1E-03	7324	431,432	New analyses in UK Biobank
Myocardial infarction						
IVW	1.03	(0.93–1.15)	5.4E-01	~61,000	~577,000	Hartiala et al.[14]
Egger regression[a]	1.14	(1.03–1.25)	7.8E-03	~61,000	~577,000	Hartiala et al.[14]
Stroke						
IVW	1.03	(0.94–1.13)	5.0E-01	40,585	406,111	Malik et al.[15]
Egger regression[a]	1.13	(0.99–1.30)	7.8E-02	40,585	406,111	Malik et al.[15]
Ischemic stroke						
IVW	1.05	(0.95–1.16)	3.2E-01	34,217	406,111	Malik et al.[15]

Inverse-variance weighted (IVW) Mendelian randomization. Estimated causal effects of circulating sclerostin genetically predicted by 10 variants in the *B4GALNT3* gene region on estimated bone mineral density (eBMD), femoral neck BMD (FN-BMD), fracture risk, myocardial infarction risk, stroke risk, and ischemic stroke risk. Betas in SD for BMD parameters and odds ratios (OR) and 95% CI for fracture risk, myocardial infarction, stroke, and ischemic stroke are given per SD increase of sclerostin. [a]Egger intercept was significant and therefore the slope given from the Egger regression should be considered.

Table 1: **Estimated causal effects of circulating sclerostin genetically predicted by variants in the *B4GALNT3* gene region on eBMD, FN-BMD, fracture risk, myocardial infarction risk, and stroke risk.**

GC for 4 weeks, resulting in a substantial bone loss (Fig. 4a). This GC-induced bone loss was associated with reduced *B4galnt3* expression in cortical bone (Fig. 4b) and increased circulating levels of sclerostin (Fig. 4c) while *Sost* expression in bone was not affected (Fig. 4d). Dexamethasone treatment reduced *B4galnt3* expression in cultured calvarial osteoblasts (Fig. 4e), supporting a direct GC-induced regulation of *B4galnt3* in osteoblast-lineage cells. These findings demonstrate that GC regulates *B4GALNT3* in osteoblast-lineage cells and one may speculate that this will result in reduced LDN-glycosylation of sclerostin and, thereby, increased sclerostin action in bone, contributing to GC-induced bone loss (Fig. 4f).

Reduced cortical bone mass and strength in *B4galnt3*$^{-/-}$ mice

A functional role of B4GALNT3 for bone mass regulation is supported by findings from the high throughput International Mouse Phenotyping Consortium (IMPC) screening program of total body BMD as analysed by DXA, revealing some evidence of reduced BMD in mice devoid of *B4galnt3* (P = 0.06, https://www.mousephenotype.org/data/genes/). We extended those preliminary high throughput skeletal analyses by evaluating not only total body BMD, but also bone site-specific (lumbar spine and femur) BMD using DXA as well as the cortical and trabecular bone compartments separately using computed tomography and bone strength using three-point bending in the *B4galnt3*$^{-/-}$ mouse model used in the present study (Fig. 4g–q). DXA analyses revealed that female *B4galnt3*$^{-/-}$ mice had reduced total body (–10.1%, P = 0.002, two-sided Student's t test), lumbar spine (–13.0%, P = 0.019%, two-sided Student's t test) and total femoral BMD (–8.9%, P = 0.004, two-sided Student's t test) compared with *B4galnt3*$^{+/+}$ mice (Fig. 4g–i). Analyses using computed tomography revealed reduced cortical bone mass in the mid-diaphyseal area of tibia (Fig. 4j–n), while the trend of reduced trabecular bone volume fraction in the vertebrae did not reach statistical significance (Fig. 4o, P = 0.09, two-sided Student's t test) in female *B4galnt3*$^{-/-}$ mice compared with *B4galnt3*$^{+/+}$ mice. In tibia, no difference in trabecular bone volume fraction was observed between *B4galnt3*$^{-/-}$ and WT mice (Fig. 4p). The bone strength (maximal load at failure) as analysed by three-point bending test in the humerus diaphyseal region (Fig. 4q) was reduced in *B4galnt3*$^{-/-}$ mice compared with *B4galnt3*$^{+/+}$ mice. Reduction of cortical bone mass in the tibia was also observed in male mice (Supplemental Table S6). Thus, *B4galnt3*$^{-/-}$ mice have reduced BMD mainly because of reduced cortical bone mass, resulting in reduced bone strength. When evaluating the association between serum sclerostin and cortical bone area in the tibia of *B4galnt3*$^{-/-}$ mice and WT mice, we observed a significant inverse association (r_s = –0.50, P = 0.018, n = 22, Spearman correlation analysis).

The expressions of the evaluated WNT signalling genes (*Axin2*, *Lef1*, *Tcf7*, and *Cyclin D1*) were not significantly altered in the cortical bone of *B4galnt3*$^{-/-}$ mice compared with WT mice, suggesting that a new steady state of WNT signalling had occurred in the 13-wk-old *B4galnt3*$^{-/-}$ mice with already reduced cortical bone area (Supplemental Table S2). In a similar

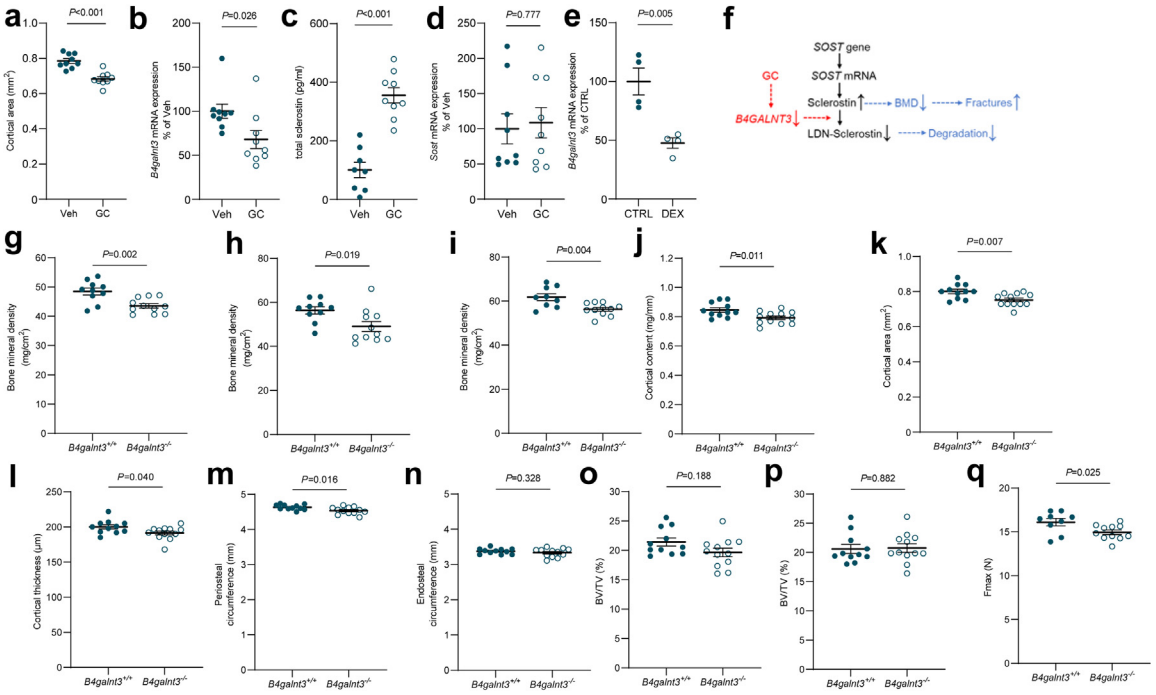

Fig. 4: **Hormonal regulation of *B4galnt3* expression in bone and reduced cortical bone mass and strength in *B4galnt3*$^{-/-}$ mice.** a–d) Cortical area of femur (a), *B4galnt3* mRNA expression in cortical bone (b), total serum sclerostin levels (c), and *Sost* mRNA expression in cortical bone (d), in 16-wk-old wildtype female mice treated with glucocorticoids (GC; n = 9, open circle) or vehicle (Veh; n = 9, filled circle) for four weeks. e) *B4galnt3* mRNA expression in primary calvarial osteoblastic cells cultured in osteogenic media for 48 h, with and without 100 nM dexamethasone (DEX). f) Proposed mechanism of hormonal regulation of B4GALNT3 and effects on LDN-glycosylation of sclerostin (LDN-Sclerostin). g–i) Areal bone mineral density (BMD) of total body (g), lumbar spine (L2–L5) (h), and whole femur (i), of 5-wk-old female *B4galnt3*$^{-/-}$ (n = 11) and *B4galnt3*$^{+/+}$ (n = 10) mice. j–n) Cortical content (j), cortical area (k), cortical thickness (l), periosteal circumference (m), and endosteal circumference (n), of tibia in 13-wk-old female *B4galnt3*$^{-/-}$ (n = 12) and *B4galnt3*$^{+/+}$ (n = 11) mice. o and p) Trabecular bone volume over total volume (BV/TV) of vertebra (o) and tibia (p) in 13-wk-old female *B4galnt3*$^{-/-}$ (n = 12) and *B4galnt3*$^{+/+}$ (n = 11) mice. q) Maximal load at failure (N) of humerus as measured by three-point-bending in 13-wk-old female *B4galnt3*$^{-/-}$ (n = 11) and *B4galnt3*$^{+/+}$ (n = 9) mice. Statistical analyses were performed using two-sided Student's *t* test. Values are given as means ± SEM.

manner, no or only modest effect on the expression of WNT signalling genes has been observed in most previous studies of different mouse models with sclerostin overexpression.[44,45]

We also measured several transcripts previously associated with calcification in aorta,[46–49] without observing any significant difference in expression in aorta between *B4galnt3*$^{-/-}$ mice and *B4galnt3*$^{+/+}$ mice (Supplemental Figure S7).

Discussion

Although global sclerostin inhibition increases bone mass and reduces fracture risk efficiently, there is some evidence of potential cardiovascular safety concerns and recent myocardial infarction, and stroke are currently contra-indications for treatment using global sclerostin inhibition by the approved sclerostin antibody romosozumab.[3] Therefore, there is an urgent medical need to increase understanding of the tissue-specific effects of sclerostin. In this study, we identified that the enzyme B4GALNT3 is co-expressed with sclerostin in osteocytes and that B4GALNT3 enhances LDN-glycosylation of sclerostin in osteoblast-lineage cells, as indicated by WFA-precipitation. This in turn results in reduced circulating sclerostin levels, increased bone mass and increased bone strength in mice and reduced circulating sclerostin levels, increased bone mass and decreased fracture risk in humans without increased risk of myocardial infarction or stroke. One may speculate that targeting B4GALNT3-mediated LDN-glycosylation of sclerostin separates the antifracture effects of sclerostin from its possible cardiovascular side effects.

We recently identified a trans-signal on chromosome 12 in the *B4GALNT3* gene region to be the by far strongest genetic signal for circulating sclerostin.[12] As *B4GALNT3* encodes for the enzyme beta-1,4-N-acetylgalactosaminyl-transferase 3 that transfers N-acetylgalactosamine (GalNAc) onto N-acetylglucosaminebeta-benzyl to form GalNAcβ1,4-GlcNAc structures to target glycoproteins (LDN-glycosylation) and sclerostin harbours two possible LDN-glycosylation sites (N53 and N175), we hypothesized

that *B4GALNT3* might be the causal gene for circulating sclerostin levels. We, therefore, developed *B4galnt3*$^{-/-}$ mice that had substantially increased circulating sclerostin levels and reduced degree of LDN-glycosylation of sclerostin. As circulating sclerostin is only osteocyte-derived[10] and we demonstrated that the intra-cellularly acting enzyme B4GALNT3 is co-localized with SOST in osteocytes, it is likely that the elevated circulating sclerostin levels in *B4galnt3*$^{-/-}$ mice is caused by a lack of B4GALNT3-mediated LDN-glycosylation of sclerostin in osteocytes. This notion is supported by our findings that overexpression of *B4galnt3* increased, while silencing of *B4galnt3* decreased, WFA-recognized LDN-glycosylation of sclerostin in cultured human osteoblast-like cells. Normal *Sost* mRNA levels were observed in bone of *B4galnt3*$^{-/-}$ mice, demonstrating that the B4GALNT3-mediated regulation of circulating sclerostin is not caused by a transcriptional regulation of *Sost* in late osteoblasts/osteocytes. Sclerostin protein levels, identified by immunoreactivity in cortical osteocytes, were increased in *B4galnt3*$^{-/-}$ mice compared with WT mice.

These results indicate that LDN-glycosylation of sclerostin enhances local degradation of sclerostin in bone, which is the sole source of circulating sclerostin, and/or the clearance of sclerostin from the circulation. Terminal GalNAc structures have been shown to be bound by asialoglycoprotein receptor (ASGP-R) expressed in hepatocytes and thereby increase the clearance of endogenous and therapeutic LDN-glycosylated glycoproteins.[50,51] One may speculate that sclerostin without LDN-glycosylation will have an increased serum half-life due to reduced hepatic clearance. Future studies are warranted to determine the effect of B4GALNT3-mediated LDN-glycosylation on local sclerostin degradation in bone and on sclerostin clearance from the circulation. Besides affecting degradation/clearance of sclerostin, B4GALNT3-mediated LDN-glycosylation may affect binding of sclerostin to LRPs (low-density lipoprotein receptor-related proteins) and thereby the biological activity of sclerostin. The most studied interaction site between sclerostin and LRP6 is not glycosylated but an additional binding site was recently discovered close to one of the N-linked glycosylation sites.[52] However, *in situ* modelling indicated that the glycosylation was directed towards the solvent and not involved in binding. WFA shows a very high affinity for binding LDN structures[34] and the method used in this study of WFA-based precipitation followed by Western blotting of target protein is widely used to determine LDN-glycosylation of proteins.[33,53,54] In addition, the WFA-binding properties were successfully employed previously for histochemical and lectin column detection of LDN epitopes.[40,55] One limitation of this approach is that even if WFA shows a very high affinity for binding LDN structures (17-fold higher as for GalNAc, which in turn shows a 5-fold higher affinity as for Gal[34]), additional potential low bindings may impact the basal levels detected for the LDN-glycosylated sclerostin. This may explain why the reduction of LDN-glycosylated sclerostin in *B4galnt3*$^{-/-}$ mice was only partial using the WFA precipitation assay. Alternatively, B4GALNT4, that also has the capacity to synthesize LDN-glycosylation structures, might have partly replaced B4GALNT3 in the *B4galnt3*$^{-/-}$ mice. *B4galnt4* was expressed in the cortical bone of *B4galnt3*$^{-/-}$ mice but its expression did not differ between *B4galnt3*$^{-/-}$ and WT mice.

It is well established that inhibition of sclerostin expression or action results in a substantial increase in bone mass.[56–58] However, like *B4galnt3*$^{-/-}$ mice with elevated sclerostin levels, several transgenic mouse models overexpressing sclerostin only display a modest reduction in bone mass.[44,45,59] In a similar manner, inactivation of WNT16 in osteoblast-lineage cells results in a substantial cortical bone loss,[29] while transgenic overexpression of WNT16 in osteoblasts using the procollagen type I α 1 promoter did not significantly increase cortical bone thickness.[60] Thus, it is possible that the dose–response effect of sclerostin on bone mass is normally rather saturated, meaning that an increase in sclerostin levels will only modestly reduce bone mass while a reduction of sclerostin will result in a markedly increase in bone mass. It has previously been proposed that there is a threshold of sclerostin above which bone formation is inhibited, rather than a linear relationship between sclerostin and bone formation.[45] We propose that a reduction in sclerostin levels, resulting in increased bone mass may be achieved by increased loading or an increased B4GALNT3 activity. Further studies are warranted to determine the effect of B4GALNT3 overexpression in osteocytes on bone mass. It is a limitation of the present study that no histomorphometry data is included. Besides the proposed effect of B4GALNT3 on cortical bone via a regulation of sclerostin, we cannot exclude other potential mechanisms mediating the effect on cortical bone in the *B4galnt3*$^{-/-}$ mice.

MR using genetic instruments as exposures often accurately predicts the beneficial effects and the possible off-target side effects of pharmaceutical targets.[3,61] One MR study, using genetic variants in the *SOST* gene as exposure, revealed that the *SOST* SNPs alleles that display the strongest association with increased bone mass and reduced fracture risk also associate with increased risk of myocardial infarction.[3] We observed that the expression of both *Sost* and *B4galnt3* are relatively high in bone while *Sost* but not *B4galnt3* expression is high in arteries. We, therefore, hypothesized that targeting B4GALNT3 might exert bone-specific effects without cardiovascular side effects. To test this hypothesis, we performed MR, demonstrating that decreased circulating sclerostin, genetically predicted by several variants in the *B4GALNT3* gene, is causally associated with increased BMD and decreased risk of fractures but

not with increased risk of myocardial infarction or stroke. As regards myocardial infarction, MR Egger analyses revealed that the Egger intercept was significant, and the Egger slope that then should be considered revealed a significant direct association between sclerostin levels genetically predicted by variants in the *B4GALNT3* gene region and risk of myocardial infarction. This finding suggests that besides increasing BMD and reducing fracture risk, targeting B4GALNT3 may reduce (and clearly not increase) the risk of myocardial infarction. Thus, the risk of myocardial infarction might be in opposite directions for elevated BMD caused by genetic variants in *B4GALNT3* compared with elevated BMD caused by genetic variants in *SOST*. A bone-specific effect of targeting B4GALNT3 is supported by our findings that *B4galnt3*$^{-/-}$ mice are apparently healthy except for a reduction of cortical bone mass and bone strength.

Glucocorticoid therapy is widely used for the treatment of various diseases, including autoimmune and inflammatory disorders and malignancies, but therapeutic use is also associated with bone loss and substantially increased risk of fractures.[62,63] GC-induced bone loss was in the present study associated with increased bone-derived circulating sclerostin levels and reduced *B4galnt3* but unchanged *Sost* expression in bone. Based on these findings, we speculate that reduced post-translational LDN-glycosylation may partly contribute to GC-induced bone loss. However, further studies are required to directly determine if GC-treatment affects sclerostin glycosylation and it should be emphasized that there are many alternative pathways independent of sclerostin by which GC may cause bone loss.

In conclusion, we identify B4GALNT3 as a key factor for bone physiology via regulation of LDN-glycosylation of sclerostin in osteoblast-lineage cells. We propose that B4GALNT3 may be a bone-specific osteoporosis target, separating the anti-fracture effect of global sclerostin inhibition, from indicated cardiovascular side effects.

Contributors

SMS, JV, JHT, UHL, PH, and CO designed the study and experiments. MN, JHT, and CO performed human genetic association studies. SMS, KHN, JW, KH, MKL, and PH performed animal experiments. LL performed *in situ* hybridization. JV, TTDL, IA, and PH performed cell culture experiments. AK and JT performed mechanical strength measurements. SMS and KHN had direct access and verified data from the animal experiments. JV and IA had direct access and verified data from the LDN-glycosylation measurements. CO and MN had direct access and verified data from the human studies. SMS, JV, KHN, JHT, UHL, PH, and CO interpreted the results. SMS, KHN, UHL, PH, and CO wrote the manuscript. All authors reviewed and edited the manuscript.

Data sharing statement

Data supporting the findings of this study are present in the paper and/or the Supplementary Materials. Additional data related to this paper may be requested from the authors.

Declaration of interests

CO has two patents/patent applications in the field of probiotics and bone health. All other authors declare that they have no conflict of interest.

Acknowledgements

We thank Anna Westerlund and Ulrika Björklund at the University of Gothenburg for excellent technical assistance. Single cell data analysis was performed by Sanna Abrahamsson from the Bioinformatics Core Facility at the Sahlgrenska Academy. This study was supported by the Swedish Research Council (2016-01001, 2018-02921, 2020-01392, 2022-01156), the Swedish Foundation of Strategic Research (FFL15-0188), the Swedish state under the agreement between the Swedish government and the county councils, the ALF agreement in Gothenburg (ALFGBG-720331, ALFGBG-965235, ALFGBG-721621, ALFGBG-965362), the IngaBritt and Arne Lundberg Foundation (LU2017-0081, LU2021-0096), the Knut and Alice Wallenberg Foundation (KAW 2015.0317), and the Novo Nordisk Foundation (NNF15OC0015080, NNF190C0055250, NNF20OC0063954). The MEGASTROKE project received funding from sources specified at http://www.megastroke.org/acknowledgements.html (Supplemental Table S7).

Appendix A. Supplementary data

Supplementary data related to this article can be found at https://doi.org/10.1016/j.ebiom.2023.104546.

References

1 Hernlund E, Svedbom A, Ivergard M, et al. Osteoporosis in the European Union: medical management, epidemiology and economic burden. A report prepared in collaboration with the International Osteoporosis Foundation (IOF) and the European Federation of Pharmaceutical Industry Associations (EFPIA). *Arch Osteoporos*. 2013;8(1):136.
2 Johnell O, Kanis JA. An estimate of the worldwide prevalence and disability associated with osteoporotic fractures. *Osteoporos Int*. 2006;17(12):1726–1733.
3 Bovijn J, Krebs K, Chen CY, et al. Evaluating the cardiovascular safety of sclerostin inhibition using evidence from meta-analysis of clinical trials and human genetics. *Sci Transl Med*. 2020;12(549):eaay6570.
4 Cosman F, Crittenden DB, Adachi JD, et al. Romosozumab treatment in postmenopausal women with osteoporosis. *N Engl J Med*. 2016;375(16):1532–1543.
5 McClung MR, Grauer A, Boonen S, et al. Romosozumab in postmenopausal women with low bone mineral density. *N Engl J Med*. 2014;370(5):412–420.
6 Holdsworth G, Staley JR, Hall P, et al. Sclerostin downregulation globally by naturally occurring genetic variants, or locally in atherosclerotic plaques, does not associate with cardiovascular events in humans. *J Bone Miner Res*. 2021;36(7):1326–1339.
7 De Mare A, Opdebeeck B, Neven E, D'Haese PC, Verhulst A. Sclerostin protects against vascular calcification development in mice. *J Bone Miner Res*. 2022;37(4):687–699.
8 Poole KE, van Bezooijen RL, Loveridge N, et al. Sclerostin is a delayed secreted product of osteocytes that inhibits bone formation. *FASEB J*. 2005;19(13):1842–1844.
9 Robling AG, Niziolek PJ, Baldridge LA, et al. Mechanical stimulation of bone in vivo reduces osteocyte expression of Sost/sclerostin. *J Biol Chem*. 2008;283(9):5866–5875.
10 Yee CS, Manilay JO, Chang JC, et al. Conditional deletion of Sost in MSC-derived lineages identifies specific cell-type contributions to bone mass and B-cell development. *J Bone Miner Res*. 2018;33(10):1748–1759.
11 Didangelos A, Yin X, Mandal K, Baumert M, Jahangiri M, Mayr M. Proteomics characterization of extracellular space components in the human aorta. *Mol Cell Proteomics*. 2010;9(9):2048–2062.
12 Zheng J, Maerz W, Gergei I, et al. Mendelian randomization analysis reveals a causal influence of circulating sclerostin levels on bone mineral density and fractures. *J Bone Miner Res*. 2019;34(10):1824–1836.
13 Morris JA, Kemp JP, Youlten SE, et al. An atlas of genetic influences on osteoporosis in humans and mice. *Nat Genet*. 2019;51(2):258–266.
14 Hartiala JA, Han Y, Jia Q, et al. Genome-wide analysis identifies novel susceptibility loci for myocardial infarction. *Eur Heart J*. 2021;42(9):919–933.

15 Malik R, Chauhan G, Traylor M, et al. Multiancestry genome-wide association study of 520,000 subjects identifies 32 loci associated with stroke and stroke subtypes. *Nat Genet*. 2018;50(4):524–537.
16 Collins R. What makes UK Biobank special? *Lancet*. 2012;379(9822):1173–1174.
17 Zhou W, Zhao Z, Nielsen JB, et al. Scalable generalized linear mixed model for region-based association tests in large biobanks and cohorts. *Nat Genet*. 2020;52(6):634–639.
18 Nethander M, Quester J, Vandenput L, Ohlsson C. Association of genetically predicted serum estradiol with risk of thromboembolism in men: a mendelian randomization study. *J Clin Endocrinol Metab*. 2021;106(8):e3078–e3086.
19 Machiela MJ, Chanock SJ. LDlink: a web-based application for exploring population-specific haplotype structure and linking correlated alleles of possible functional variants. *Bioinformatics*. 2015;31(21):3555–3557.
20 Luo S, Au Yeung SL, Zhao JV, Burgess S, Schooling CM. Association of genetically predicted testosterone with thromboembolism, heart failure, and myocardial infarction: mendelian randomisation study in UK Biobank. *BMJ*. 2019;364:l476.
21 Davies NM, Holmes MV, Davey Smith G. Reading Mendelian randomisation studies: a guide, glossary, and checklist for clinicians. *BMJ*. 2018;362. k601.
22 Burgess S, Dudbridge F, Thompson SG. Combining information on multiple instrumental variables in Mendelian randomization: comparison of allele score and summarized data methods. *Stat Med*. 2016;35(11):1880–1906.
23 Bowden J, Davey Smith G, Burgess S. Mendelian randomization with invalid instruments: effect estimation and bias detection through Egger regression. *Int J Epidemiol*. 2015;44(2):512–525.
24 Burgess S, Zuber V, Valdes-Marquez E, Sun BB, Hopewell JC. Mendelian randomization with fine-mapped genetic data: choosing from large numbers of correlated instrumental variables. *Genet Epidemiol*. 2017;41(8):714–725.
25 Greco MF, Minelli C, Sheehan NA, Thompson JR. Detecting pleiotropy in Mendelian randomisation studies with summary data and a continuous outcome. *Stat Med*. 2015;34(21):2926–2940.
26 Lallemand Y, Luria V, Haffner-Krausz R, Lonai P. Maternally expressed PGK-Cre transgene as a tool for early and uniform activation of the Cre site-specific recombinase. *Transgenic Res*. 1998;7(2):105–112.
27 Gergei I, Zheng J, Andlauer TFM, et al. GWAS meta-analysis followed by Mendelian randomization revealed potential control mechanisms for circulating alpha-Klotho levels. *Hum Mol Genet*. 2022;31(5):792–802.
28 Ohlsson C, Nilsson KH, Henning P, et al. WNT16 overexpression partly protects against glucocorticoid-induced bone loss. *Am J Physiol Endocrinol Metab*. 2018;314(6):E597–E604.
29 Moverare-Skrtic S, Henning P, Liu X, et al. Osteoblast-derived WNT16 represses osteoclastogenesis and prevents cortical bone fragility fractures. *Nat Med*. 2014;20(11):1279–1288.
30 Vidal O, Lindberg MK, Hollberg K, et al. Estrogen receptor specificity in the regulation of skeletal growth and maturation in male mice. *Proc Natl Acad Sci U S A*. 2000;97(10):5474–5479.
31 Windahl SH, Vidal O, Andersson G, Gustafsson JA, Ohlsson C. Increased cortical bone mineral content but unchanged trabecular bone mineral density in female ERbeta(-/-) mice. *J Clin Invest*. 1999;104(7):895–901.
32 Sato T, Gotoh M, Kiyohara K, et al. Molecular cloning and characterization of a novel human beta 1,4-N-acetylgalactosaminyltransferase, beta 4GalNAc-T3, responsible for the synthesis of N, N'-diacetyllactosediamine, galNAc beta 1-4GlcNAc. *J Biol Chem*. 2003;278(48):47534–47544.
33 Hsu WM, Che MI, Liao YF, et al. B4GALNT3 expression predicts a favorable prognosis and suppresses cell migration and invasion via beta(1) integrin signaling in neuroblastoma. *Am J Pathol*. 2011;179(3):1394–1404.
34 Haji-Ghassemi O, Gilbert M, Spence J, et al. Molecular basis for recognition of the cancer glycobiomarker, LacdiNAc (GalNAc [beta1–>4]GlcNAc), by Wisteria floribunda agglutinin. *J Biol Chem*. 2016;291(46):24085–24095.
35 Voelkl J, Tuffaha R, Luong TTD, et al. Zinc inhibits phosphate-induced vascular calcification through TNFAIP3-mediated suppression of NF-kappaB. *J Am Soc Nephrol*. 2018;29(6):1636–1648.
36 Nilsson KH, Henning P, El Shahawy M, et al. RSPO3 is important for trabecular bone and fracture risk in mice and humans. *Nat Commun*. 2021;12(1):4923.
37 Henning P, Moverare-Skrtic S, Westerlund A, et al. WNT16 is robustly increased by oncostatin M in mouse calvarial osteoblasts and acts as a negative feedback regulator of osteoclast formation induced by oncostatin M. *J Inflamm Res*. 2021;14:4723–4741.
38 Matsushita Y, Nagata M, Kozloff KM, et al. A Wnt-mediated transformation of the bone marrow stromal cell identity orchestrates skeletal regeneration. *Nat Commun*. 2020;11(1):332.
39 Granholm S, Henning P, Lindholm C, Lerner UH. Osteoclast progenitor cells present in significant amounts in mouse calvarial osteoblast isolations and osteoclastogenesis increased by BMP-2. *Bone*. 2013;52(1):83–92.
40 Ikehara Y, Sato T, Niwa T, et al. Apical Golgi localization of N,N'-diacetyllactosediamine synthase, beta4GalNAc-T3, is responsible for LacdiNAc expression on gastric mucosa. *Glycobiology*. 2006;16(9):777–785.
41 Gotoh M, Sato T, Kiyohara K, et al. Molecular cloning and characterization of beta1,4-N-acetylgalactosaminyltransferases IV synthesizing N,N'-diacetyllactosediamine. *FEBS Lett*. 2004;562(1–3):134–140.
42 Tikhonova AN, Dolgalev I, Hu H, et al. The bone marrow microenvironment at single-cell resolution. *Nature*. 2019;569(7755):222–228.
43 Sato AY, Cregor M, Delgado-Calle J, et al. Protection from glucocorticoid-induced osteoporosis by anti-catabolic signaling in the absence of Sost/sclerostin. *J Bone Miner Res*. 2016;31(10):1791–1802.
44 Rhee Y, Allen MR, Condon K, et al. PTH receptor signaling in osteocytes governs periosteal bone formation and intracortical remodeling. *J Bone Miner Res*. 2011;26(5):1035–1046.
45 Tu X, Rhee Y, Condon KW, et al. Sost downregulation and local Wnt signaling are required for the osteogenic response to mechanical loading. *Bone*. 2012;50(1):209–217.
46 Sattler AM, Schoppet M, Schaefer JR, Hofbauer LC. Novel aspects on RANK ligand and osteoprotegerin in osteoporosis and vascular disease. *Calcif Tissue Int*. 2004;74(1):103–106.
47 Tacey A, Qaradakhi T, Brennan-Speranza T, Hayes A, Zulli A, Levinger I. Potential role for osteocalcin in the development of atherosclerosis and blood vessel disease. *Nutrients*. 2018;10(10):1426.
48 Lok ZSY, Lyle AN. Osteopontin in vascular disease. *Arterioscler Thromb Vasc Biol*. 2019;39(4):613–622.
49 Alexopoulos A, Bravou V, Peroukides S, et al. Bone regulatory factors NFATc1 and Osterix in human calcific aortic valves. *Int J Cardiol*. 2010;139(2):142–149.
50 Uhler R, Popa-Wagner R, Kroning M, et al. Glyco-engineered HEK 293-F cell lines for the production of therapeutic glycoproteins with human N-glycosylation and improved pharmacokinetics. *Glycobiology*. 2021;31(7):859–872.
51 Baenziger JU, Fiete D. Galactose and N-acetylgalactosamine-specific endocytosis of glycopeptides by isolated rat hepatocytes. *Cell*. 1980;22(2 Pt 2):611–620.
52 Kim J, Han W, Park T, et al. Sclerostin inhibits Wnt signaling through tandem interaction with two LRP6 ectodomains. *Nat Commun*. 2020;11(1):5357.
53 Che MI, Huang J, Hung JS, et al. β1, 4-N-acetylgalactosaminyltransferase III modulates cancer stemness through EGFR signaling pathway in colon cancer cells. *Oncotarget*. 2014;5(11):3673–3684.
54 Nakane T, Angata K, Sato T, Kaji H, Narimatsu H. Identification of mammalian glycoproteins with type-I LacdiNAc structures synthesized by the glycosyltransferase B3GALNT2. *J Biol Chem*. 2019;294(18):7433–7444.
55 Kitamura N, Guo S, Sato T, et al. Prognostic significance of reduced expression of beta-N-acetylgalactosaminylated N-linked oligosaccharides in human breast cancer. *Int J Cancer*. 2003;105(4):533–541.
56 Li X, Ominsky MS, Niu QT, et al. Targeted deletion of the sclerostin gene in mice results in increased bone formation and bone strength. *J Bone Miner Res*. 2008;23(6):860–869.
57 Lin C, Jiang X, Dai Z, et al. Sclerostin mediates bone response to mechanical unloading through antagonizing Wnt/β-catenin signaling. *J Bone Miner Res*. 2009;24(10):1651–1661.
58 Krause C, Korchynskyi O, de Rooij K, et al. Distinct modes of inhibition by sclerostin on bone morphogenetic protein and Wnt signaling pathways. *J Biol Chem*. 2010;285(53):41614–41626.
59 Loots GG, Kneissel M, Keller H, et al. Genomic deletion of a long-range bone enhancer misregulates sclerostin in Van Buchem disease. *Genome Res*. 2005;15(7):928–935.

60 Moverare-Skrtic S, Wu J, Henning P, et al. The bone-sparing effects of estrogen and WNT16 are independent of each other. *Proc Natl Acad Sci U S A*. 2015;112(48):14972–14977.
61 Ference BA, Holmes MV, Smith GD. Using mendelian randomization to improve the design of randomized trials. *Cold Spring Harb Perspect Med*. 2021;11(7):a040980.
62 Canalis E, Mazziotti G, Giustina A, Bilezikian JP. Glucocorticoid-induced osteoporosis: pathophysiology and therapy. *Osteoporos Int*. 2007;18(10):1319–1328.
63 van Staa TP, Leufkens HG, Cooper C. The epidemiology of corticosteroid-induced osteoporosis: a meta-analysis. *Osteoporos Int*. 2002;13(10):777–787.